Theoretical study of size-dependent properties of BN nanotubes with intrinsic defects

G. Y. Gou,[1] B. C. Pan,[1,2,*,†] and L. Shi[1,*,‡]

[1]*Hefei National Laboratory for Physical Sciences at Microscale, University of Science and Technology of China, Hefei, Anhui 230026, People's Republic of China*

[2]*Department of Physics, University of Science and Technology of China, Hefei, Anhui 230026, People's Republic of China*

(Received 25 June 2007; revised manuscript received 7 September 2007; published 17 October 2007)

Intrinsic defects in zigzag BN nanotubes, including single vacancy, divacancy, and Stone-Wales defects, are systematically investigated using density functional calculation. It is found that the structural configurations and formation energies of the topological defects in considered tubes are dependent on tube diameter. The results demonstrate that such size-dependent properties are originated from the strong curvature effect in BN nanotubes. Furthermore, the scanning tunneling microscope images of intrinsic defects in the BN nanotubes are predicted.

DOI: 10.1103/PhysRevB.76.155414 PACS number(s): 61.46.Fg, 61.72.Ji, 71.15.Nc, 73.22.−f

I. INTRODUCTION

Soon after the discovery of carbon nanotubes (CNTs),[1] one of their isoelectronic structures, boron nitride nanotubes (BNNTs), have been predicted by theoretical calculation[2] and synthesized experimentally[3,4] later on. Different from CNTs, BNNTs are semiconductors with a large band gap of about 5.8 eV,[5] weakly dependent on the diameter (tube size) and chirality of the tube,[6] and, thus, exhibit outstanding chemical inertness.[7] Such a unique property will make them an excellent candidate in technological applications for possible nanoscale optical and luminescent devices.

Similar to CNTs, BN nanotubes are usually not defect free. Experimental observations showed that the B or N atoms could be removed under electron irradiation, leaving behind vacancies,[8] BN divacancies, or even extended topological defects.[9] In addition, the Stone-Wales defects were predicted to be formed in BNNTs under large tension.[10,11] Basically, the existence of these topological defects should influence the electronic and mechanical properties of nanotubes[12,13] to some extent. For example, previous theoretical calculations of isolated intrinsic defects[14,15] clearly indicated that the electronic structures of the BNNTs could be modified by the existing defects. It is noted that the theoretical effort was restricted to the (10,0) tube only, where size effects (or diameter effects) of the tube, which are the fundamental issues related to the physical nature of defective tubes,[16] were not considered in their publication.

In this paper, the structural features and stabilities of the single vacancies, divacancies, and Stone-Wales defects in BN nanotubes with different diameters were comprehensively studied using density functional calculation. It is found that the calculated formation energies and local geometries of these defects are size dependent. It is further demonstrated that their size-dependent properties are originated from the curvature effect of the tubes. Moreover, the scanning tunneling microscope (STM) images of the intrinsic defects in BNNTs are predicted.

II. METHODOLOGY

Our calculations were carried out using the local spin density functional formulism implemented in the SIESTA code.[17–19] The norm conserving pseudopotentials generated using the Troullier-Martins scheme[20] were employed to describe the interaction of valence electrons, which were expressed in the fully separable form developed by Kleinman and Bylander.[21] A double-zeta basis set was employed in all calculations to represent the valence wave functions. The generalized gradient approximation correction in the form of Perdew-Burke-Ernzerhof[22] was adopted for the exchange-correlation potential. Spin-unrestricted density functional theory was used to obtain all the results reported below. A set of four Monkhorst-Pack[23] special k points along the tube axis was used to sample the Brillouin zone.

Since it has been experimentally[24] and theoretically verified[25] that the BN nanotubes are dominated by zigzag (n, 0) type, a series of zigzag tubes (n ranges from 6 to 15) are employed in the present work.

All calculations have been performed in the periodic boundary condition, with supercells three times the primary cell along the tube axis for single vacancy defects, and four times for divacancies and Stone-Wales defects. The spacing between the tubes in their lateral directions were set to be at least 7 Å. This supercell configuration assures that defects are isolated from each other. The conjugate gradient algorithm[26] was adopted to fully relax the structures of the nanotubes until the maximum of forces acting on the atoms was no more than 0.04 eV/Å.

III. RESULTS AND DISCUSSION

A. Structures and stabilities

For convenience, the (8, 0) tube is firstly selected for our study. A single vacancy defect (V_B or V_N) is obtained by removing a B or N atom from a perfect tube, a divacancy (DV) is generated by removing a pair of B-N atoms along the tube axis, and a Stone-Wales (SW) defect is created by rotating an axial B-N bond by $\pi/2$. The fully relaxed configurations of the four defects are presented in Fig. 1.

For an ideal single vacancy of either V_B or V_N, there are three dangling bonds (3DBs) in the vacancy region. Similar to CNTs,[16] such a local vicinity of DBs has a possibility to rebond two of the dangling-bond atoms due to the lattice deformation induced by curvature. After full relaxation, the

ideal V_N defect transforms into a 5-1DB (local atomic network around the point defect features one pentagon and one DB) configuration spontaneously, whereas the initial structure with three DBs of the V_B still remains. For this case, by moving two of three DBs closer, it is found that the resulting geometry also characterizes a 5-1DB configuration, where there is a newly formed N-N bond perpendicular to the tube axis.[27] Basically, B and N atoms in a BN tube are inequivalent to each other. So, the single vacancies of B and N atoms should characterize different structural features. After examining the resulting structures for the single vacancies of both V_B and V_N [Figs. 1(a) and 1(b)], it is found that unlike the case of V_N, the DB atom moves much more outward from the initial tube surface and there is a shorter homoatomic bond in the V_B defect.

We now proceed to comparatively analyze the relative stabilities of the defects studied above. For this purpose, we calculated the formation energy of a defected BN nanotube. The formation energy is defined as

$$E_{form} = E_{binding}[\text{defected}] - E_{binding}[\text{ideal}],$$

$$E_{binding} = E_{total} - n_B\mu_B - n_N\mu_N, \quad (1)$$

where E_{total} and $E_{binding}$ are total energy and binding energy of a given system. μ_B, μ_N are chemical potentials for B, N atoms, respectively, which are taken from the calculated energies of their isolated atoms. By definition, $E_{form} > 0$ corresponds to an endothermal procedure for the formation of a defect.

The calculated formation energies and geometrical parameters (bond lengths of homoatomic bonds) of the local defects in (8,0) tube are summarized in Table I. As shown in Table I, the obtained formation energies of the relevant defects are consistent with the reported results from previous publication,[28] which verifies the reliability of the methodology employed in the present work.

When considering a vacancy pair, the combined formation energies of two separate single vacancies (V_B and V_N) in a (8,0) tube is about 6.4 eV higher than that of the DV, which indicates that the separate single vacancies of V_B and V_N in a tube tend to merge together. Such a preferable combination of single vacancies is mainly driven by eliminating the DBs of the two 5-1DB defects.[9] In addition, the bond lengths of B-B and N-N bonds in the DV are 1.72 and 1.48 Å, respectively, which are shorter than those in the respective single vacancies (as seen in Table I), just reflecting the enhancement of the interaction between these atoms and the gain in energy to some extent.

As for a SW defect, it does not possess any dangling bond, and the bond lengths (1.70 Å for a B-B bond and 1.49 Å for a N-N bond) around the defect region bear a little deviation over the average of the original hexagon network (1.44 Å). As a consequence, it introduces the least lattice distortion among all the defects discussed above and, thus, well preserves the sp^2 bonding character of the original lattice network. Therefore, the SW defect has the lowest formation energy[29] among the defects mentioned above.

In order to explore the size-dependent features of these defects in their relative stabilities and local geometries, the calculations are extended to all other considered $(n, 0)$ tubes. The bond lengths of homoatomic bonds formed in each defect are employed as the geometric parameters to characterize its local geometry. Figure 2 plots the calculated formation energies and bond lengths of homoatomic bonds around local regions of V_B, V_N, and SW defects as a function of tube index n. Strikingly, the evolution of defects against tube size is characterized by two distinct features. (i) Similar formation energy curves for all defects are observed: as the tube size increases, the formation energy of any considered defect increases monotonously at a small $(n=6-8)$ or large size $(n=13-15)$, while it exhibits an odd-even evolution in the moderate size range $(n=9-12)$. (ii) The different evolution tendencies of the local geometries are found: the evolution of local structures around single vacancies is well correlated to their formation energy curves; however, bond lengths for SW defect slightly decrease with the increase of tube diameter, which deviate from its energy trends.

The evolution of formation energies and the concerned bond lengths with tube diameter as mentioned above do couple with the bonding character. Basically, like the case of CNTs, the electronic and mechanical properties for BNNTs

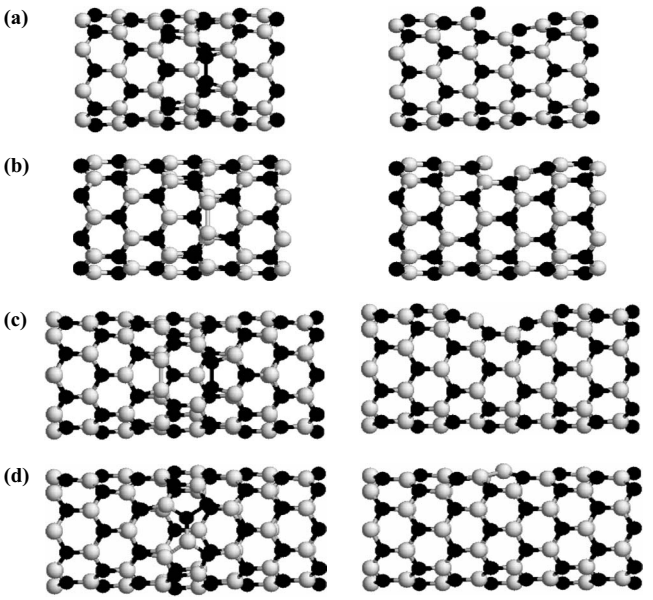

FIG. 1. Top view (left) and side view (right) of optimized structures of (a) V_B, (b) V_N, (c) DV, and (d) SW defects in (8,0) tube. White (black) balls represent B (N) atoms.

TABLE I. Calculated and reference values (Ref. 28) of formation energies (in eV) of four kinds of defects and bond lengths (in Å) of homoatomic bonds in (8,0) tube.

Defect	E_{form} (This work)	E_{form} (Ref. 28)	Bond length B-B	Bond length N-N
V_B	14.83	14.21		1.492
V_N	11.60	11.57	1.806	
DV	20.01		1.721	1.477
SW	5.02	4.68	1.704	1.493

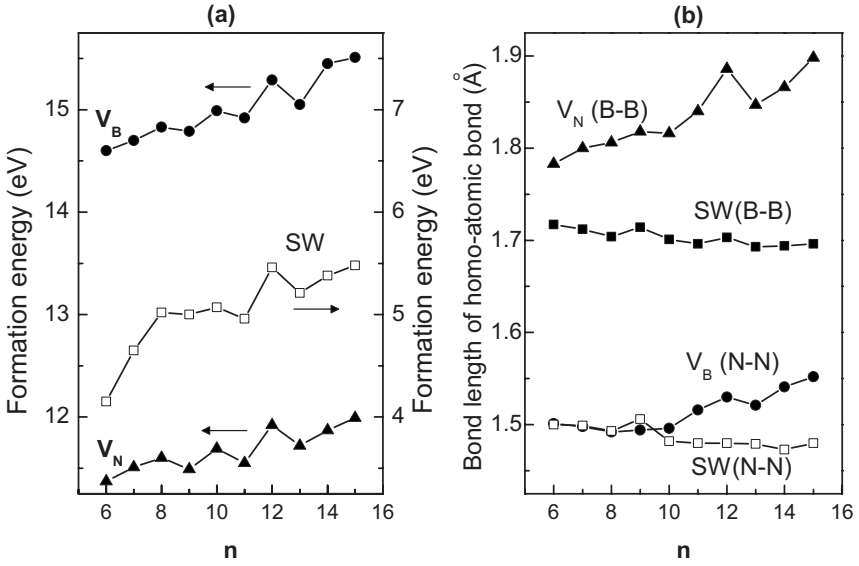

FIG. 2. (a) Formation energies and (b) bond lengths of homoatomic bonds as a function of tube index n for V_B (filled circle), V_N (triangle), and SW (filled square or empty square), respectively.

with small size can be significantly different from their large-sized counterpart,[6,30,31] which is mainly attributed to the $\sigma-\pi$ rehybridization due to the large curvature of the tube. For a tube containing a topological defect, the defect gives rise to more or less lattice distortion, changing the hybrid character of an ideal tube to some extent.[14]

In the case of a single vacancy defect, the original sp^2-like bonding character around the vacancy is distorted, causing additional constraints. These constraints can be reduced by forming a new homoatomic bond in the vacancy region. The strength of this bond is enhanced by decreasing the tube diameter. Therefore, the formation energy of the 5-1DB defect in a BNNT with a smaller diameter is lower than that with a larger diameter. However, such a situation does not appear in the case of the SW defect. Instead, the bond lengths of both B-B and N-N bonds at the SW defect decrease very slightly as the diameter of the tube increases. Therefore, it is hard to concisely couple the strengths of these bonds with the formation energy trend in the SW defect. Then, we turn to calculate the bond length deviation Δl to evaluate how a SW defect affects the network of the tube. Here, $\Delta l=\bar{l}-\bar{l}_0$, $\bar{l}_0$ and $\bar{l}$ are the average bond lengths of a perfect tube and B-N bonds around the SW defect region, respectively. The bond length deviation as a function of the tube index n is displayed in Fig. 3, where it is found that the positive bond length deviation decreases with increasing tube size. Based on the results obtained above, it is inferred that the SW defect tends to release the radial strain induced by curvature by expanding the local defect region. The extent of expansion can be uniquely characterized by bond length deviation. Particularly, this phenomenon becomes significant for small-sized tube with enormous curvature effect. The larger the curvature is, the greater the extent of the radial strain that can be released by the SW defect, thereby accompanied by a larger bond length deviation.[32] As a result, the system gains more energy, further enhancing its stability.

Thus, it is concluded that the different bonding characters of single vacancies and SW defects lead to the distinct local structure evolution, while the similar formation energy trends imply that both systems are mainly dominated by a strong curvature effect in their size-dependent features.

On the other hand, similar to the perfect tubes,[6] there should be a threshold value of diameter beyond which the curvature effect can be neglected and the defected tube properties behave insensitively to the tube size. This behavior is characterized in our results by the tendencies of formation energies and local structures in defective tubes to become stationary as the tube size increases. Combining Figs. 2 and 3, the threshold of tube diameter is estimated to be larger than 10.2 Å ($n>13$). The smallest single-wall BN tubes experimentally available average at 1.4 nm in their diameters[33] ($n_{av}=18$ for zigzag tubes), while for the most abundantly produced samples, the average tube diameters may go far beyond the threshold size. Thus, we propose that their defective behaviors are characterized by size-independent features. These results demonstrate the insensitivity of the optical and electronic modulation effects on tube size by the introduction of intrinsic defects in BNNTs.

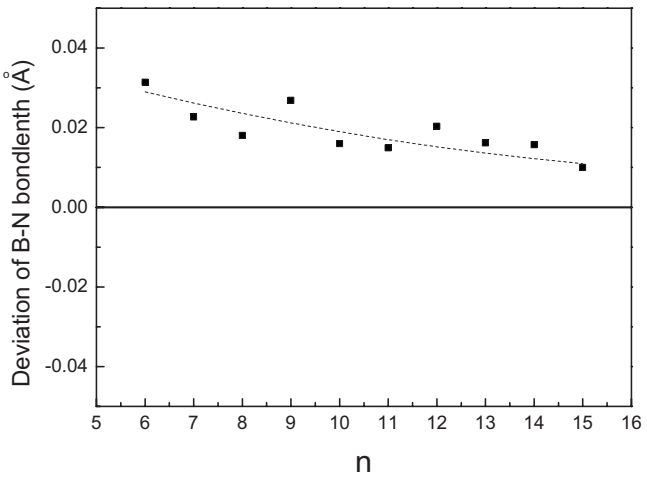

FIG. 3. The bond length deviation of B-N bond at the SW defect as a function of tube index n. The dashed line is for guiding the eyes.

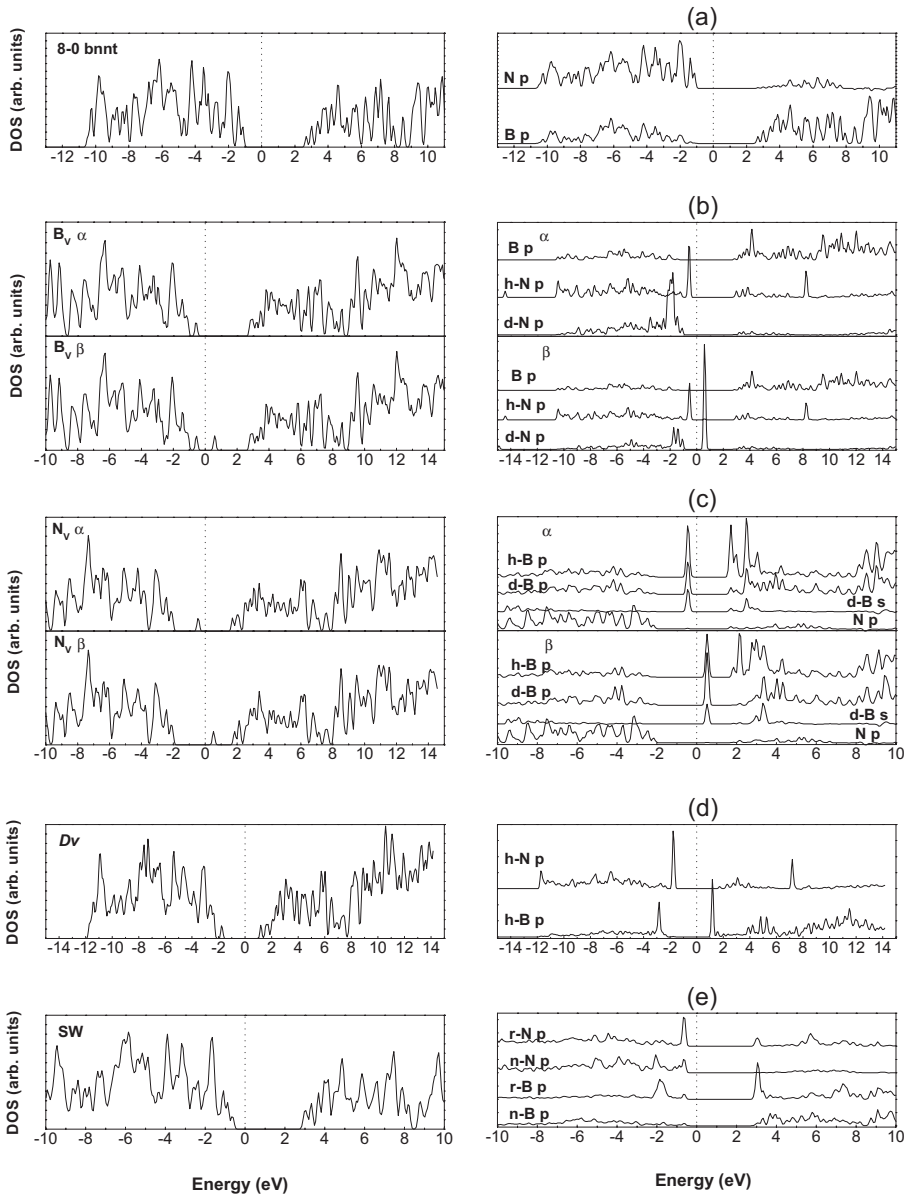

FIG. 4. DOS (left) and LDOS (right) of BNNTs: (a) ideal, (b) V_B, (c) V_N, (d) DV, and (e) SW defected (8,0) tubes. Majority and minority spin electronic density of states for V_B and V_N are distinguished with α and β labels, respectively. Fermi levels presented as dotted lines are at 0.0 eV. (The labels used for specific atoms in LDOS are described in the main text.)

B. Electronic structures

To gain deep insight into defective zigzag BNNTs, the electronic structures are studied. Total density of states (DOS) and local density of states (LDOS) for ideal and defective (8,0) BNNTs are described in Fig. 4, where the density of states for both α and β electrons (spin up and down) are given for open shell systems (V_B and V_N). In the LDOS of an ideal tube [Fig. 4(a)], it is found that the states at the top of the valence band are mostly contributed by the N atoms, while the states at the bottom of the conduction band are from the B atoms, which is essentially ascribed to the ionic nature of the B-N bond.[34] In the case of the defected systems, the defects of single vacancies and divacancy introduce additional states within the gap region, reducing the band gap width effectively. Moreover, the corresponding energy bands of these defective states are a little dispersed over the Brillouin zone in their band structures, implying their localized properties in the energy landscape.

In detail, the V_B defect introduces the spin double degenerate occupied states at 0.55 eV below the Fermi level and the unoccupied states at 0.59 eV above the Fermi level, where the former is mainly contributed by $2p$ electrons of homoatomic bonded N atoms (h-N) and the latter from the $2p$ electron of the dangling-bond atom N (d-N) [Fig. 4(b)]. Moreover, Mulliken population analysis shows that the total net spin ($S=1/2$) mainly comes from the unpaired electron at d-N atom. In the case of V_N defect, there are two spin splitting defective states in the gap region, as illustrated in Fig. 3(c). The occupied and unoccupied energy levels are symmetrically centered around the Fermi level, donated by both dangling-bond and homoatomic bonded B (d-B and h-B) atoms. Further, by Mulliken analysis, we find that, distinct from that of V_B, the unpaired electrons are contributed by both d-B and h-B atoms in V_N defect. The s electrons also contribute to V_N gap states, indicating the different hybrid

features of atoms in the defect region between V_B and V_N defects.

The electronic structures of DV defect are quite different from those of the single vacancies, since they are spin degenerate. The shallow states introduced by DV are contributed by $2p$ electrons of homoatomic B-B and N-N (h-B and h-N) atoms separately [see Fig. 4(d)]. By analysis of Mulliken population, we find that homoatomic bonds in DV are actually a pair of oppositely charged defect centers. The strong interaction between them results in a large energy splitting between highest occupied molecular orbital and lowest unoccupied molecular orbital from defective states.

Unlike the case of the vacancies, there are no obvious gap states arising from the SW defects. As compared with the related ideal tubes, no reduction of band gap in SW defective tubes are observed. This can be understood from the fact that SW topological defect well preserves the sp^2 bonding character of the original lattice network, due to the least lattice distortion introduced. Particularly, in Fig. 4(e), we find that $2p$ states from the atoms at the center of the SW defect (B and N atoms at the rotated bond, marked as r-B and r-N) mainly concentrate at band edges, while the LDOS of other atoms including the nearest neighbor atoms (n-B and n-N) to the rotated bond are not significantly altered from their equivalence in perfect tubes. Therefore, the change of electronic states are only contributed by the rotated bond in the case of the SW defect. Overall, the SW defect in a BN tube results in some change in electronic properties compared to the corresponding perfect BNNT.

It was reported that SW defects in BN tubes exhibit localized modification in their STM images.[10] Actually, the electronic states arising from the vacancies are more localized than those in the SW defects. Therefore, the localized features of the vacancies in BNNTs may be reflected in their STM images too. We thus simulate the STM images of the topological defects mentioned above in BN nanotubes based on the approximation given by Tersoff and Hamann.[35] In the STM simulations, a constant height of 7–8 bohr is used to simulate the spacing between the tip and the defective region in the tube. The calculated STM images with different bias voltages for defective (8,0) BNNTs are presented in Fig. 5.

First of all, we calculate the STM images of the SW defect. The simulated images characterize N-N π and B-B π^* features with −1.5 and +3.5 V bias voltages, respectively. The main aspects of the obtained STM images are qualitatively consistent with previous results.[10]

The STM images for the V_B defect are obtained with applied bias voltages of −0.85 and +3.0 V, respectively. It is observed that the occupied states feature a dumbbell-like shape (ppπ-like states), located at the homoatomic bond, while the unoccupied states are presented as bright speckles (σ^* states), located at the dangling-bond atom.

For the V_N defect, the STM images at ±0.8 V clearly exhibit the defective states located within the gap region. These images are characterized by trianglelike spots centered at the 5-1DB defect region for both occupied and unoccupied defective states, implying that the π-character covalent bond is formed around the defect region.

In the case of the DV defect, the localized defective states can be clearly extracted in its STM images under bias voltages of −2.0 and +1.5 V. The π- and π^*-like states locate around homoatomic N-N and B-B bonds, respectively, which are spatially separated from each other.

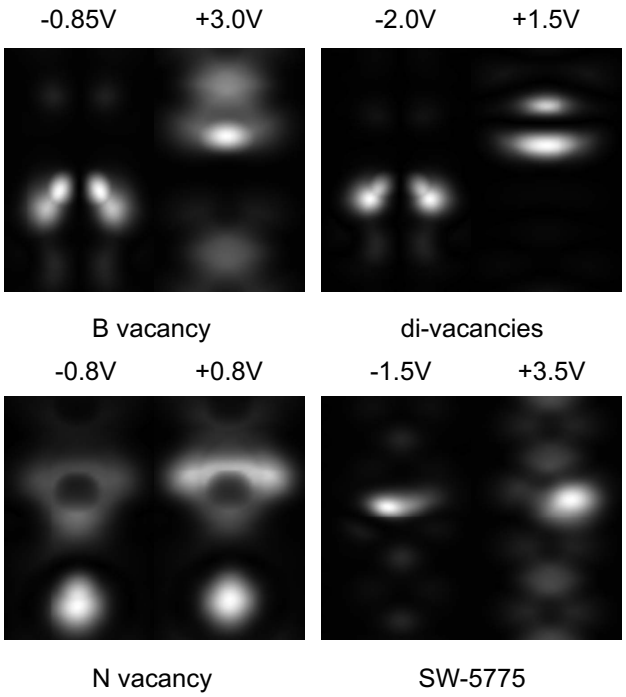

FIG. 5. Simulated STM images for (8,0) tubes with individual V_B, V_N, DV, or SW defect under bias voltages, respectively.

Our results reveal that different intrinsic defects can create a uniquely localized modification of the STM image as compared to perfect tubes,[36] and therefore, topological defects in BNNTs can be unambiguously detected by STM measurements.

IV. CONCLUSION

Based on *ab initio* calculations, the structures and electronic properties of BNNTs with intrinsic defects of B vacancy, N vacancy, divacancies, and Stone-Wales are systematically investigated. It is found that the formation energies and geometries around the local defect for all studied defects are size dependent, dominated by a strong curvature effect. Moreover, defective tubes at large size behave as stationary electronic and optical properties independent of tube diameter. In addition, by simulating STM images of defective tubes, the uniquely localized modification of each defect is found in their STM images, which could be used as the fingerprint for experimental identification of point defects in BNNTs complemented with a STM probe.

ACKNOWLEDGMENTS

This work is financially supported by the Ministry of Science and Technology of China (NKBRSF-G1999064603), National Basic Research Program of China (2006CB922000), and National Science Foundation of China (Grants No. 10174071 and No. 10574115). The HP-LHPC of USTC is acknowledged for computational support.

*Corresponding authors.
†bcpan@ustc.edu.cn
‡shil@ustc.edu.cn

[1] S. Iijima, Nature (London) **354**, 56 (1991).
[2] A. Rubio, J. L. Corkill, and M. L. Cohen, Phys. Rev. B **49**, 5081 (1994).
[3] N. G. Chopra, R. J. Luyken, K. Cherrey, V. H. Crespi, M. L. Cohen, S. G. Louie, and A. Zettl, Science **269**, 966 (1995).
[4] A. Loiseau, F. Willaime, N. Demoncy, G. Hug, and H. Pascard, Phys. Rev. Lett. **76**, 4737 (1996).
[5] R. Arenal, O. Stéphan, M. Kociak, D. Taverna, A. Loiseau, and C. Colliex, Phys. Rev. Lett. **95**, 127601 (2005).
[6] X. Blase, A. Rubio, S. G. Louie, and M. L. Cohen, Europhys. Lett. **28**, 335 (1994).
[7] Y. Chen, J. Zhou, S. J. Campell, and G. L. Caer, Appl. Phys. Lett. **84**, 2430 (2004).
[8] R. S. Lee, J. Gavillet, M. Lamy de la Chapelle, A. Loiseau, J.-L. Cochon, D. Pigache, J. Thibault, and F. Willaime, Phys. Rev. B **64**, 121405 (2001).
[9] A. Zobelli, C. P. Ewels, A. Gloter, G. Seifert, O. Sténphan, S. Csillag, and C. Colliex, Nano Lett. **6**, 1955 (2006).
[10] Y. Miyamoto, A. Rubio, S. Berber, M. Yoon, and D. Tománek, Phys. Rev. B **69**, 121413(R) (2004).
[11] H. F. Bettinger, T. Dumitrică, G. E. Scuseria, and B. I. Yakobson, Phys. Rev. B **65**, 041406(R) (2002).
[12] X. D. Bai, D. Golberg, Y. Bando, C. Y. Zhi, C. C. Tang, M. Mitome, and K. Kurashima, Nano Lett. **7**, 632 (2007).
[13] P. H. Zhang and V. H. Crespi, Phys. Rev. B **62**, 11050 (2000).
[14] T. M. Schmidt, R. J. Baierle, P. Piquini, and A. Fazzio, Phys. Rev. B **67**, 113407 (2003).
[15] P. Piquini, R. Baierle, T. M. Schmidt, and A. Fazzio, Nanotechnology **16**, 827 (2005).
[16] A. J. Lu and B. C. Pan, Phys. Rev. Lett. **92**, 105504 (2004).
[17] P. Ordejón, E. Artacho, and J. M. Soler, Phys. Rev. B **53**, R10441 (1996).
[18] D. Sánchez-Portal, P. Ordejón, E. Artacho, and J. M. Soler, Int. J. Quantum Chem. **65**, 453 (1997).
[19] J. M. Soler, E. Artacho, J. D. Gale, A. García, J. Junquera, P. Ordejón, and D. Sánchez-Portal, J. Phys.: Condens. Matter **14**, 2745 (2002).
[20] N. Troullier and J. L. Martins, Phys. Rev. B **43**, 1993 (1991).
[21] L. Kleinman and D. M. Bylander, Phys. Rev. Lett. **48**, 1425 (1982); M. Bylander and L. Kleinman, Phys. Rev. B **41**, 907 (1990).
[22] J. P. Perdew, K. Burke, and M. Ernzerhof, Phys. Rev. Lett. **77**, 3865 (1996); **78**, 1396 (1997).
[23] H. J. Monkhorst and J. D. Pack, Phys. Rev. B **13**, 5188 (1976).
[24] R. Arenal, M. Kociak, A. Loiseau, and D.-J. Miller, Appl. Phys. Lett. **89**, 073104 (2006).
[25] H. J. Xiang, J. L. Yang, J. G. Hou, and Q. S. Zhu, Phys. Rev. B **68**, 035427 (2003).
[26] W. H. Press, B. P. Flannery, S. A. Teukolsky, and W. T. Vetterling, *New Numerical Recipes* (Cambridge University Press, New York, 1986).
[27] The full optimization of V_B with a pentagon and weakly formed monoatomic N-N bond tilted to the tube axis (5-1DB-T) shows that this kind of defect is unstable. 5-1DB-T geometry is available only at smaller tube radius (formation energy about 1 eV larger than the 5-1DB case) due to higher curvature. At relatively large size ($n>7$), the monoatomic bond forced by hand at the initial stage dissociates automatically.
[28] X. J. Wu, J. L. Yang, J. G. Hou, and Q. S. Zhu, J. Chem. Phys. **121**, 8481 (2004).
[29] T. Dumitrică, H. F. Bettinger, G. E. Scuseria, and B. I. Yakobson, Phys. Rev. B **68**, 085412 (2003).
[30] X. Blase, L. X. Benedict, E. L. Shirley, and S. G. Louie, Phys. Rev. Lett. **72**, 1878 (1994).
[31] X. Blase, A. DeVita, J. C. Charlier, and R. Car, Phys. Rev. Lett. **80**, 1666 (1998).
[32] B. C. Pan, W. S. Yang, and J. L. Yang, Phys. Rev. B **62**, 12652 (2000).
[33] J. S. Lauret, R. Arenal, F. Ducastelle, A. Loiseau, M. Cau, B. Attal-Tretout, E. Rosencher, and L. Goux-Capes, Phys. Rev. Lett. **94**, 037405 (2005).
[34] K. H. Khoo, M. S. C. Mazzoni, and S. G. Louie, Phys. Rev. B **69**, 201401(R) (2004).
[35] J. Tersoff and D. R. Hamann, Phys. Rev. Lett. **50**, 1998 (1983).
[36] M. Ishigami, J. D. Sau, S. Aloni, M. L. Cohen, and A. Zettl, Phys. Rev. Lett. **97**, 176804 (2006).